Intermingled basins due to finite accuracy

Malte Schmick*
Max-Planck-Institut für molekulare Physiologie, Postfach 500247, 44202 Dortmund, Germany

Eric Goles†
Center for Mathematical Modelling of Complex Systems, FCFM–Universidad de Chile, Casilla 170-3, Santiago, Chile

Mario Markus‡
Max-Planck-Institut für molekulare Physiologie, Postfach 500247, 44202 Dortmund, Germany
(Received 10 January 2000)

We investigate numerically first a chaotic map interrupted by two small neighborhoods, each containing an attracting point, and secondly a periodically tilted box within which disorderly colliding disks can reach different attracting configurations, due to dissipation. For finite, arbitrarily small accuracy, both systems have basins of attraction that are indistinguishable from intermingled basins: any neighborhood of a point in phase space leading to one attractor contains points leading to the other attractor. A bifurcation destabilizing the fixed points or the disk configurations causes on-off intermittency; the disks then alternate between a ''frozen'' and a gaslike state.

PACS number(s): 05.45.−a, 68.35.Rh, 47.52.+j, 02.70.Ns

Riddled and intermingled basins received considerable attention in the last few years [1–14]. Such basins impose serious restrictions on predictability. In fact, an increase in accuracy of the initial conditions is not of much help in improving predictions, as compared to the less severe chaotic systems, in which predictions can be improved by decreasing initial errors. Moreover, the unpredictability resulting from riddled or intermingled basins affects our knowledge of its qualitative fate, i.e., we cannot predict the attractor (it may be periodic or chaotic), while the unpredictability in a chaotic system refers only to the knowledge of the position in phase space within the chaotic attactor.

Given the basins B_1 and B_2 of two coexisting attractors, B_1 is said to be riddled with respect to B_2 if the probability of reaching B_1 is positive and if within any neighborhood of any point of B_1 the probability of reaching B_2 is also positive. This means that an arbitrarily small perturbation of a point leading to one attractor may lead to the other attractor. This property has been found for a number of time-discrete systems [2,5–7], electronic circuits [8,9], differential equations describing a point mass in a potential [1,3,4], coupled Roessler systems [11], or coupled elastic arches [10]. As a special case, the basins are said to be intermingled if B_1 is riddled with respect to B_2, and B_2 is riddled with respect to B_1 [2–4].

In a recent report, it was shown that, for chaotic transients, appearing close to a so-called boundary crisis, there exist time-dependent riddledlike basins for finite, arbitrarily small accuracy; this apparent riddling is indistinguishable from riddled basins owing to the unavoidable limitations in computational or experimental accuracy [12]. In that report, however, riddling appears only if one evaluates the system for a finite time since the basins are transients and there exists only one attractor for $t\to\infty$. In contrast, we show in the present work that there exist systems for which riddled basins caused by finite accuracy are not a transient phenomenon; in fact, riddling can be quantified for two attractors coexisting at $t\to\infty$. Moreover, the basins reported now are not only riddled, as in Ref. [12], but intermingled. It is also interesting that the coexisting attractors in the present work are fixed points or periodic orbits, in contrast to previous works in which at least one attractor is chaotic (an exception involving nonchaotic attractors, as in our systems, is given by a recent report [6] on riddling of a mixed type, i.e., riddled basins intertwined with open sets).

A quantitative description of riddling is possible with the so-called uncertainty exponent α [3,5,7,10,12–14]. α is determined by fitting the scaling law $f(\epsilon)\propto\epsilon^{\alpha}$, where $f(\epsilon)$ is the fraction of pairs $(\vec{x}_k,\vec{x}_k+\vec{\epsilon}_r)$ such that $\vec{x}_k$ and $\vec{x}_k+\vec{\epsilon}_r$ are in different basins. The $\vec{x}_k, k=1,2,\ldots,N$ are initial conditions (chosen equidistantly in this work) and the $\vec{\epsilon}_r$ are perturbations chosen randomly such that $|\vec{\epsilon}_r|$ is uniformly distributed within $[0,\epsilon]$. For riddled or intermingled basins, α is close to zero. Examples of reported values are in the range $0.01\leqslant\alpha\leqslant 0.03$ [5,10,13], as compared to $0.4\leqslant\alpha\leqslant 0.7$ for fractal basins [15] and $\alpha=1$ if the basin boundary is a smooth curve or surface [15].

As a simple system, chosen so as to easily understand the phenomenon, we use a map that corresponds to the logistic equation except for two small intervals $I_i=[X_i-\delta,X_i+\delta], i=1,2, \delta\ll 1$:

$$x_{n+1}=\begin{cases} sx_n+(1-s)X_i & \text{if } x_n\in I_i, \quad i=1,2 \\ 4x_n(1-x_n) & \text{if } x_n\in\,]0,1[\text{ and } x_n\notin I_i. \end{cases} \tag{1}$$

For $|s|>1$, X_1 and X_2 are unstable and the map is chaotic. For $|s|\leqslant 1$ and starting at a point $x_0\notin I_i$, the map eventually

*Electronic address: schmick@mpi-dortmund.mpg.de
†Electronic address: egoles@dim.uchile.cl
‡Electronic address: markus@mpi-dortmund.mpg.de

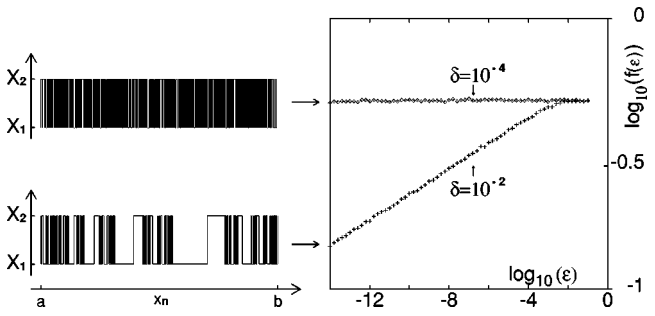

FIG. 1. Right: Plot for the determination of the uncertainty exponent $|d\log_{10}f(\epsilon)/d\log_{10}\epsilon|$ with the map given by Eq. (1), $s=0$. Left: Examples of basins corresponding to the plots at the right (abscissas: $a=0.9$, $b=0.901$; ordinates: coexisting attractors $X_1=0.2$ and $X_2=0.8$).

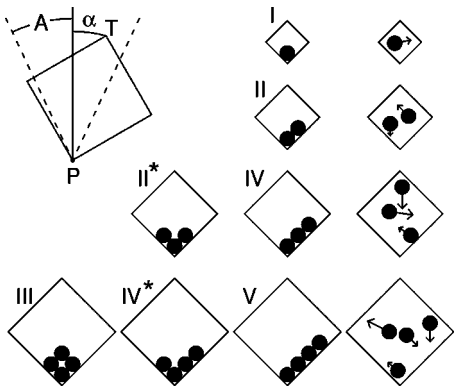

FIG. 2. Upper left: Scheme of the mechanical device; the point T oscillates around the pivot P between the dashed lines; $\alpha=A\cos(2\pi ft)$. Smaller squares: possible stable configurations with one disk (top row), two disks (second row), three disks (third row), and four discs (lowest row); the disordered modes are illustrated in the right column; the other modes (periodic orbits) are denoted by roman numerals.

gets ''trapped'' into one of the I_i and converges there to the corresponding attractor X_i. In this work, we set $X_1=0.2$ and $X_2=0.8$. Since $\delta\ll 1$, the map may spend a considerable time as a chaotic transient, which is defined by the logistic equation, before the trapping into one of the I_i occurs. All preimages of I_i, as determined by this chaotic transient, are contained in the basin of the X_i. Since the Lyapunov exponent of the map (1) is $\lambda=1$, the average length of a preimage of the I_i is $\delta\times 2^{-m}$, where m is the number of backward iterations. For a calculational accuracy ξ (here $\xi=10^{-16}$), the preimages of the I_i will be indistinguishable from points for $m\geqslant m_c=\ln(\delta/\xi)/\ln(2)$. As an example, we now consider $\delta=10^{-4}$. In that case, $m_c=41$, well below the average number of iterations needed to reach the I_i by the chaotic map, which is of the order 10^3. We determined the total length of all preimages of the I_i between 1 and m_c backward iterations to be $L\approx 10^{-3}$. We thus conclude for $\delta=10^{-4}$ that approximately 99.9% of the initial conditions consist of points from the numerical point of view.

It is known that the set of all preimages of a point in]0,1[resulting from $m\to\infty$ backward iterations of the map $x_{n+1}=4x_n(1-x_n)$ is dense in]0,1[(see, e.g., [16]); thus, any subinterval of]0,1[contains preimages of two arbitrarily chosen points. This property suggests (for finite m and I_i, as is our case) that the preimages of I_1 are highly intertwined with those of I_2. We found numerically that this intertwining is so strong for $\delta=10^{-4}$ that successive enlargements of subintervals of]0,1[, as far as computational accuracy allowed, revealed no open subsets of the basins; we thus obtained qualitative evidence for intermingling. We show an example for the analysis of a subinterval of]0,1[in this case in the upper left of Fig. 1. Note that some subsets of the displayed interval look open. However, closer inspection showed that this is due to the limited number of points examined in this interval; in fact, enlargement of these seemingly open sets again reveals an intertwined structure. A quantitative analysis yielded the upper plot at the right of Fig. 1. This plot confirms the scaling law $f(\epsilon)\propto\epsilon^{\alpha}$ with $\alpha=0.0025\pm 0.0001$ for $\delta=10^{-4}$. For comparison, the lower plot at the right of Fig. 1 was calculated with more extended I_i, namely, with $\delta=10^{-2}$. We obtain $L\approx 0.56$, i.e., only 44% of the unit interval appears to have intermingled basins; starting from these basins, the mean number of iterations is well above m_c, being 48 in this case. We show part of this basin at the lower left of Fig. 1. Within the open intervals in this basin, neighboring points lead to the same attractor, thus decreasing $f(\epsilon)$. However, for $\epsilon\gtrsim 10^{-3}$, the evaluated point pairs are sufficiently often in different basins, again yielding $\alpha\approx 0$, i.e., apparent intermingling. Note that ϵ corresponds here to the resolution of the procedure. This resolution can also be modified by changing the computational accuracy. If, for example, $\delta=10^{-4}$, as in the upper plots of Fig. 1, but using an accuracy of 10^{-32} instead of 10^{-16}, then $\alpha\approx 0$ for $\epsilon\gtrsim 10^{-20}$, but $\alpha>0$ for $\epsilon<10^{-20}$.

The phenomena just described apply for $|s|\leqslant 1$. If $|s|>1$, then the X_i are unstable and the iterates are repelled out of the intervals I_i. However, if $|s|-1$ is sufficiently close to zero, the iterates may spend considerable time intervals of duration τ in the I_i, with $\tau\to\infty$ for $|s|\to 1$. Note that exit from the I_i is described by $(x_{n+1}-X_i)=s(x_n-X_i)$. Thus, if the I_i is entered at the iteration k and the lifetime within I_i is τ, then $(x_{k+\tau}-X_i)=s^{\tau}(x_k-X_i)$. This equation, along with the condition for exit ($|x_{k+\tau-1}-X_i|<\delta<|x_{k+\tau}-X_i|$) and the assumption that the probability of reaching any $x_k\in I_i$ is $p(x_k)\approx$ const (since $I_i\ll 1$), yields the scaling law $p(\tau)\propto s^{-\tau}$ for $\tau\to\infty$; $p(\tau)$ is the probability for exit within τ iterations. This scaling is not comparable to any of the known laws for intermittency (see [18]), the discrepancy being due to the discontinuities of our map.

We consider now a physical system, namely, a (two-dimensional) square box containing ν disks (radius R) and oscillating around a pivot P, as illustrated in the upper left of Fig. 2. In the present work, we consider $\nu=1,2,3$, and 4. The length of the edge of the box was set to $2R(\nu+1)$. This choice resulted from the consideration that a smaller box considerably restricts the movement of the disks, while a larger box diminishes the number of collisions and thus reduces the disordering that is necessary for intermingling. This disordering can still be accomplished with longer edges by increasing the input power; however, this requires unreasonably long computing times.

The straight line passing through P and the top point T describes an angle $\alpha=A\cos(2\pi ft)$ with a vertical line passing trough P. Due to dissipation, the disks may come to rest

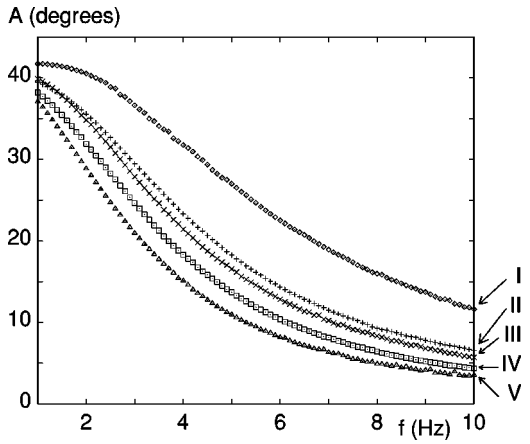

FIG. 3. A (ordinate) is the amplitude and f (abscissa) is the frequency of the oscillating box in the upper left of Fig. 2. The configurations shown in Fig. 2 are stable below the curve with the corresponding roman numeral. (The curves for II and IV deviate by less than 2% from the curves for II* and IV*, respectively.)

at one of the configurations I, II, II*, III, IV, IV* and V shown in Fig. 2. At sufficiently large A or f, disorder is maintained, as illustrated in the right column of Fig. 2.

The system illustrated in Fig. 2 was simulated using two-dimensional molecular dynamics [17]. Each disk was described by five independent variables: position $\vec{r}_i$, velocity $\vec{v}_i$, and magnitude of the angular velocity $|\vec{\omega}_i|$. For the material properties of the disks and the disk-disk and the disk-edge interactions, we used the same parameters and force laws as in [19] and [20]. In accordance with the simulations in those works, which were optimized so as to fit experimental observations, we make the following assumptions. The radii of the disks are set here to $R=5\times10^{-3}$ m and their density ρ to 2.5×10^{3} kg/m^{-3}. Two disks i and j only interact if the overlap $\zeta=2R-|\vec{r}_i-\vec{r}_j|>0$. The repulsive normal force is given by

$$\vec{F}_n^{(i)}=[Y\xi^{3/2}-\gamma_n\sqrt{\zeta}(\vec{v}_i-\vec{v}_j)\vec{n}]\vec{n} \tag{2}$$

(Hertz theory with viscoelastic dissipation [21]) with $\vec{n}=(\vec{r}_i-\vec{r}_j)/|\vec{r}_i-\vec{r}_j|$. The disk stiffness is set to $Y=10^5$ kg m$^{-1/2}$ s^{-2} and the damping constant to $\gamma=30$ kg m$^{-1/2}$ s^{-1}. The shear force (perpendicular to $\vec{n}$) is

$$\vec{F}_s^{(i)}=-\frac{\vec{v}_s}{|\vec{v}_s|}\min(\nu_s|\vec{F}_n^{(i)}|,\gamma_s|\vec{v}_s|). \tag{3}$$

The first argument describes the Coulomb sliding friction and the second one the viscous flow. The shear velocity is $\vec{v}_s=\vec{v}_i-\vec{v}_j-[(\vec{v}_i-\vec{v}_j)\vec{n}]\vec{n}+r_p\vec{n}\times(\vec{\omega}_i+\vec{\omega}_j)$. $\gamma_s=20$ kg s^{-1}; $\nu_s=0.45$. The interaction of a disk i with an edge was computed by assuming a disk placed symmetrically to i with respect to that edge. The equations were solved by a Gear predictor-corrector algorithm [17] of sixth order with a time step of 10^{-5} s.

Figure 3 shows the plane defined by the control parameters A and f. The configurations (defined in Fig. 2 and indicated by roman numerals at each curve) are unstable above the corresponding curve and stable below it. Symmetric configurations (obtained by interchanging left with right edges of the box) are considered as equivalent in Figs. 2 and 3. We found that the stability curves (Fig. 3) for the configurations IV and II are the same as those that for the configurations IV* and II*, respectively, within an error $<2\%$. This is due to the fact that instability is mainly determined by growth of perturbations of the uppermost disk in the configuration, and this disk, including a neighborhood around it, is indistinguishable between IV and IV*, as well as between II and II*. Above the curve marked I, disorder is obtained for any $\nu\leqslant4$. Below the curve marked V, all configurations coexist in phase space for $\nu=1,2,3$, or 4. Between the curves marked IV and V, the configurations III and IV* (for $\nu=4$) and the configurations II* and IV (for $\nu=3$) coexist in phase space.

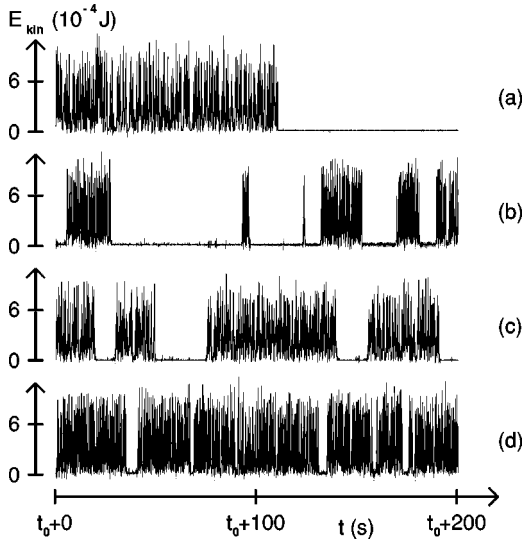

FIG. 4. Time series showing transitions between the disordered and the stable modes for two disks (second row in Fig. 2). $f=6$ Hz. Ordinate: total kinetic energy of the disks (evaluated from the velocities relative to the box). (a) $A=14.432°$, $t_0=0$; the parameters are below the curve marked II in Fig. 3; after a long chaotic transient, the disks stabilize into configuration II. (b), (c), (d) $t_0=200$ s; intermittent time series for parameters above the curve marked II in Fig. 3: increasing A decreases the mean lengths of time intervals in which the disks are ''frozen'' near configuration II. (b) $A=14.445°$; (c) $A=14.455°$; (d) ($E_{\rm kin}\approx0$) $A=14.52°$.

Slightly below each curve in Fig. 3, we observed long chaotic transients before the configuration marked at the curve was reached. This is illustrated in Fig. 4(a) and is comparable to the behavior of the one-dimensional (1D) map given by Eq. (1) for $|s|\leqslant1$. In the same way as for the 1D map, the chaotic transients here cause neighboring initial conditions to reach different attractors. This is illustrated for $\nu=4$ in Figs. 5(a), 5(b), and 5(c) for cases (with $f=3.25$ Hz) in which the configurations III and IV* coexist. The initial conditions are set by first putting the disks in configuration V and then displacing the uppermost disk along the edge [as given by the abscissas in Figs. 5(a), 5(b), and 5(c)] and perpendicularly to the edge (as given by the ordinates in these figures). In the case of Fig. 5(a), A is so small and thus transient chaos is so short that the sizes of the basins are well above calculational accuracy, thus appearing as open sets. This is an analogous situation to that for the 1D map, as illustrated at the lower left of Fig. 1.

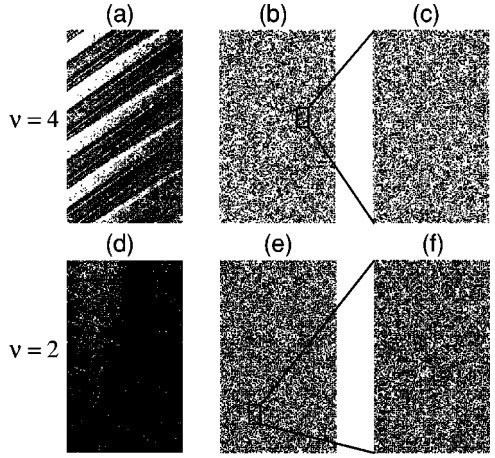

FIG. 5. (a),(b),(c) Basins for the configurations III (black) and IV* (white) of four disks (see lowest row in Fig. 2). $f=3.25$ Hz. (a) $A=22.25°$ (open sets). (b) $A=22.5°$ (intermingledlike basin). (c) Enlargement of a small rectangle within (b). (d),(e),(f) Basin for configuration II (shown black) and of its symmetric one on the left edge (shown white). $f=3.5$ Hz. (d) $A=25°$ (one basin consists of isolated points within the other one). (e) $A=26.3°$ (intermingledlike basins). (f) Enlargement of a small rectangle within (e). (a),(b),(d),(e) Abscissa $(0,6\times10^{-5}$ m) and ordinate $(0,10^{-4}$ m) are initial displacements of one disk, as described in the text.

In the case of Fig. 5(b), A is large enough and thus transient chaos is long enough to yield basins having sizes smaller than the calculational accuracy. As for the 1D map (see the upper part of Fig. 1), one here obtains basins that cannot be distinguished from intermingled ones, as illustrated qualitatively by the enlargement in Fig. 5(c). For Fig. 5(b), we calculated the uncertainty exponent to be $\alpha=0.0035\pm0.002$ (evaluated for nine orders of magnitude $10^{-12}R<\epsilon<10^{-3}R$). We determined the maximum Lyapunov exponent λ_{max} (using base 2) by averaging over 1000 chaotic transients before their breakdown into one of the stable configurations. For this, we first normalized the variables—dividing by their averages in time—and then determined the average stretching of (periodically normalized) distances between a reference trajectory and nearby trajectories (see, e.g., [18]). We obtained $\lambda_{max}=23.24\pm0.06\ s^{-1}$. This means that a perturbation having the size of the calculational accuracy (10^{-16}) increases (on average) to $2R$ (an approximate final distance in phase space that is decisive for alternative configurations) within about 2 s. This time is approximately five times shorter than the average lifetime of the chaotic transients in this case.

Figures 5(d), 5(e), and 5(f) correspond to cases for $\nu=2$ below curve II in Fig. 3 and $f=3.5$ Hz. We investigate now the basins of the two symmetric configurations of the two disks, one at the lower right edge (II^R) and one at the lower left edge (II^L) of the box. The initial conditions were set by first shifting configuration II^R a distance $2R$ upward along the lower right edge, and then displacing the lower disk along the edge [as given by the abscissas in Figs. 5(d), 5(e), and 5(f)] and perpendicularly to the edge (as given by the ordinates in these figures). For the case of Fig. 5(d), A is so low and thus the chaotic transients so short that configuration II^R is reached for almost all initial conditions (its basin is shown black). The definition of riddling is not fulfilled in this numerical analysis because the probability of reaching II^L is indistinguishable from zero [the basin consists of the isolated white points in Fig. 5(d)]. For the case of Fig. 5(e), A is large enough and thus the chaotic transients are long enough to yield again apparent intermingling with $\alpha=0.0013\pm0.001$ (evaluated for $10^{-12}R<\epsilon<10^{-3}R$).

Slightly above each curve in Fig. 3 we obtain intermittent behavior, in which a chaotic, gaslike mode alternates in a disorderly way with a ''frozen'' state, the latter corresponding to the configuration marked on the curve. We illustrate this in Figs. 4(b), 4(c) and 4(d) for $\nu=2$. This is comparable to the dynamics of the 1D map given by Eq. (1) for $|s|>1$. Due to the high degree of disorder in the chaotic bursts, we could not discriminate well between low amplitudes of the chaotic regime and laminar periods. This resulted in unreliable statistical evaluations of small τ, and thus of $\langle\tau\rangle$. However, we could well determine the probability $p(\tau)$ for large τ. We found $p(\tau)\propto\exp[\rho(A-A_c)\tau]$ with $\rho=3.93\pm0.13\approx-4$; A_c is the critical value of A (for fixed f) above which transition to chaos occurs for $\nu=2$, as given by the curve marked II in Fig. 3. We also found such a distribution with $\rho\approx4$ for $\nu=3$ (destabilization of configuration II* above curve II in Fig. 3) and for $\nu=4$ (destabilization of configuration III above curve III in Fig. 3). These probability distributions suggest that we are dealing with a behavior related to type-II intermittency [18,22].

We thank FONDAP, Chile, for financial support.

[1] J.C. Sommerer and E. Ott, Nature (London) **365**, 138 (1993).
[2] J.C. Alexander, J.A. Yorke, Z. You, and I. Kan, Int. J. Bifurcation Chaos Appl. Sci. Eng. **2**, 795 (1992).
[3] Y.-C. Lai and C. Grebogi, Phys. Rev. E **52**, 3313 (1995).
[4] J.C. Sommerer and E. Ott, Phys. Lett. A **214**, 243 (1996).
[5] Y.-C. Lai and C. Grebogi, Phys. Rev. E **53**, 1371 (1996).
[6] Y.-C. Lai and C. Grebogi, Phys. Rev. Lett. **83**, 2926 (1999).
[7] Y.C. Lai and R.L. Winslow, Phys. Rev. Lett. **72**, 1640 (1994).
[8] T. Kapitaniak and L.C. Chua, Int. J. Bifurcation Chaos Appl. Sci. Eng. **6**, 357 (1996).
[9] P. Ashwin, J. Buescu, and I. Stewart, Phys. Lett. A **193**, 126 (1994).
[10] M. Woltering and M. Markus, Phys. Lett. A **260**, 453 (1999).
[11] J.F. Heagy, T.L. Carroll, and L.M. Pecora, Phys. Rev. Lett. **73**, 3528 (1994).
[12] M. Woltering and M. Markus, Phys. Rev. Lett. **84**, 630 (2000).
[13] E. Ott, J. Sommerer, J.C. Alexander, I. Kan, and J.A. Yorke, Phys. Rev. Lett. **71**, 4134 (1993).
[14] Y.-C. Lai and R.L. Winslow, Physica D **74**, 353 (1994).
[15] S.W. McDonald, C. Grebogi, E. Ott, and J.A. Yorke, Physica D **17**, 125 (1985).
[16] M. Schroeder, *Fractals, Chaos and Power Laws* (W.H. Freeman, New York, 1991).
[17] J.M. Haile, *Molecular Dynamics Simulation* (Wiley, New York, 1992).
[18] H.G. Schuster, *Deterministic Chaos* (VCH, Weinheim, 1989).

[19] K. Kötter, E. Goles, and M. Markus, Phys. Rev. E **60**, 7182 (1999).
[20] M. Scherer, K. Kötter, M. Markus, E. Goles, and I. Rehberg, Phys. Rev. E **61**, 4069 (2000).
[21] G. Kuwabara and K. Kono, Jpn. J. Appl. Phys., Part 1 **26**, 1230 (1987).
[22] P. Bergé, Y. Pomeau, and C. Vidal, *Order Within Chaos: Towards a Deterministic Approach to Turbulence* (Hermann, Paris, 1984).